Technical University of Denmark

DTU

A-Site Deficient (Pr0.6Sr0.4)(1-s)Fe0.8Co0.2O3-delta Perovskites as Solid Oxide Fuel Cell Cathodes

Kammer Hansen, Kent

DTU Library
Technical Information Center of Denmark

A-Site Deficient $(Pr_{0.6}Sr_{0.4})_{1-s}Fe_{0.8}Co_{0.2}O_{3-\delta}$ Perovskites as Solid Oxide Fuel Cell Cathodes

K. Kammer Hansen[*,z]

Fuel Cells and Solid State Chemistry Division, Risø National Laboratory for Sustainable Energy, Technical University of Denmark, DK-4000 Roskilde, Denmark

Five A-site deficient $(Pr_{0.6}Sr_{0.4})_{1-s}Fe_{0.8}Co_{0.2}O_{3-\delta}$ perovskites ($s = 0.01$, 0.05, 0.10, 0.15, and 0.20) were synthesized using the glycine-nitrate process. The perovskites were characterized with powder X-ray diffraction (XRD), dilatometry, four-point dc conductivity measurements, and electrochemical impedance spectroscopy using cone-shaped electrodes on a $Ce_{0.9}Gd_{0.1}O_{1.95}$ electrolyte. XRD revealed that only the compounds with $s=0.01$ and 0.05 were of single phase. The other compounds contained an additional phase in the form of a Co–Fe spinel. The thermal expansion coefficient decreased systematically with an increase in s. The total conductivity followed the small polaron hopping process below a certain characteristic temperature. The total conductivity decreased with increasing s. It was likewise shown that the polarization resistance found a minimum for the compound with $s=0.05$, with a total area specific resistance more than 3 times lower than the weakly A-site deficient $(Pr_{0.6}Sr_{0.4})_{0.99}Fe_{0.8}Co_{0.2}O_{3-\delta}$ perovskite.

© 2009 The Electrochemical Society. [DOI: 10.1149/1.3194786] All rights reserved.

The solid oxide fuel cell (SOFC) is a high temperature generator of heat and electricity. One major obstacle that must be overcome, if the SOFC is to be commercialized, is lowering of the operation temperature.[1] To make this possible, new electrode materials are needed. On the cathode side Co- or Fe–Co-based electrodes have the highest activity toward the reduction of oxygen in an SOFC,[2] even though examples of other systems with an equal electrochemical activity are known.[3] In this sense two compositions have been extensively investigated in the literature, $Sm_{0.5}Sr_{0.5}CoO_{3-\delta}$ and $La_{0.6}Sr_{0.4}Fe_{0.8}Co_{0.2}O_{3-\delta}$.[4-9] An area specific resistance (ASR) of 0.18 Ω cm^2 at 600°C has been reached by a composite of $Sm_{0.5}Sr_{0.5}CoO_{3-\delta}$ and $Ce_{1-x}Gd_xO_{2-\delta}$ (CGO).[4] This is still not a high enough performance at 600°C, and better electrode materials must be developed. Recently, even better/lower ASR values have been obtained on a $Ba_{0.5}Sr_{0.5}Fe_{0.2}Co_{0.8}O_{3-\delta}$-based cathode.[10] An ASR of less than 0.1 Ω cm^2 at 600°C was obtained. However, electrodes made with this compound are not stable over time.[11,12] A few studies of A-site deficient Fe–Co-based perovskites have been reported.[13-15] It was shown that the conductivity depends on the A-site stoichiometry.[13] Likewise, it was shown that the thermal expansion coefficient (TEC) decreases when the A-site stoichiometry is lowered. From powder X-ray diffraction (XRD) it was concluded that the A-site deficient perovskites were rhombohedral and single phase.[13] Results of the electrochemistry of the A-site deficient $(La_{0.6}Sr_{0.4})_{1-s}Fe_{0.8}Co_{0.2}O_{3-\delta}$ were reported in Ref. 15. The activity was strongly dependent on s. These A-site deficient perovskites consisted of two cubic perovskite phases and one spinel phase.[15] The strongly A-site deficient perovskite $(La_{0.6}Sr_{0.4})_{0.9}Fe_{0.8}Co_{0.2}O_{3-\delta}$ has been investigated as porous composite electrodes with $Ce_{0.9}Gd_{0.1}O_{1.95}$ (CGO10) with relatively good results, as an ASR value of 0.19 Ω cm^2 was obtained on a CGO10 electrolyte at 600°C.[14] This is better than the ASR value obtained on the stoichiometric $La_{0.6}Sr_{0.4}Fe_{0.8}Co_{0.2}O_{3-\delta}$ perovskite.[9] Even though the perovskite was strongly A-site deficient, the perovskite was not stable together with yttria-stabilized zirconia.

In this study a series of A-site deficient $(Pr_{0.6}Sr_{0.4})_{1-s}Fe_{0.8}Co_{0.2}O_{3-\delta}$ perovskites ($s=0.01$, 0.05, 0.10, 0.15, and 0.20) was synthesized and investigated as SOFC cathodes by using electrochemical impedance spectroscopy (EIS) and cone-shaped electrodes. The use of cone-shaped electrodes is very convenient when studying SOFC electrodes.[15-19] The contact area of the cone-shaped electrode can be determined using Newman's formula[20]

$$r = \frac{1}{4R_s\sigma^*} \qquad [1]$$

where R_s is the intercept at the real axis at high frequency and σ^* is the specific conductivity of the electrolyte. r is the radius of the contact between the cone-shaped electrode and the electrolyte, from which the contact area can be calculated. The polarization resistance on cone-shaped electrodes is much higher than the polarization resistance on porous planar electrodes. Fe–Co-based cathodes with Pr are of particular interest as they perform better than Fe–Co-based cathodes with other A-site cations.[21]

Experimental

Synthesis of the $(Pr_{0.6}Sr_{0.4})_{1-s}Fe_{0.8}Co_{0.2}O_{3-\delta}$ perovskites was done using the glycine-nitrate route.[22] Aqueous solutions of the metal nitrates were mixed in an appropriate ratio in a beaker. Glycine was then added. The solutions were then heated on a hot plate until they ignited. The resulting powders were transferred to alumina crucibles and were calcined at 1100°C/12 h in air in a box furnace. The following starting compounds were used as metal nitrates: $Pr(NO_3)_3$ (Alfa Aesar, 99.9%), $Sr(NO_3)_2$ (Alfa Aesar, 99%), $Fe(NO_3)_3$ (Alfa Aesar, 98%), and $Co(NO_3)_2$ (Alfa Aesar, 99.8%). To evaluate the phase purity of the calcined powders, powder XRD using a Stoe θ–θ diffractometer equipped with Cu Kα radiation was performed. The diffractograms were recorded in the range 2θ: 20–80°. The bars for the dilatometry and conductivity measurements and the cylinders for the fabrication of the cone-shaped electrodes were made as follows: The powders were pressed in appropriate dies (bars and cylinders) and sintered at 1250°C/12 h in a box furnace in air. The bars were then machined into 4 × 4 × 18 mm bars and the cylinders were machined into cone-shaped electrodes. The cone-shaped electrodes had a base of 7.5 mm and sides with an angle of 45°. The density of the bars was determined with the Archimedes method. The CGO10 pellet used for the electrochemical measurements was made as follows: CGO10 powder (Rhodia) was mixed with stearic acid and glycerine in a ball mill with ethanol. After drying the powder was pressed to a disk in an appropriate die and sintered at 1500°C/2 h in air in a box furnace. The stearic acid was added as a lubricant and the glycerine was added as a binder. The dilatometry measurements were performed by using a Netzh 402 dilatometer in the temperature range of 30–1000°C with heating and cooling ramps of 2°C/min. The bars were kept at 1000°C for 2 h before cooling down. The four-point dc conductivity measurements were also performed in air using a Keithley micro-ohmmeter together with a personal computer (PC) controlling the ohmmeter and the furnace temperature. An in-house PC Linux program, was used for the collection of the data (temperature and resistance). The

---

* Electrochemical Society Active Member.
z E-mail: kkha@risoe.dtu.dk
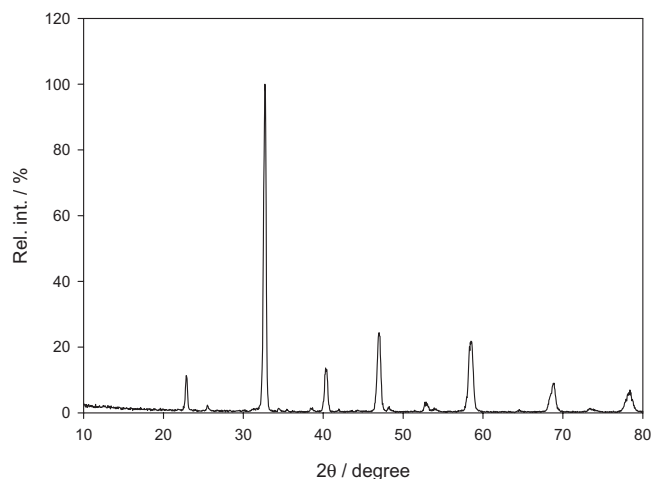
Figure 1. Powder XRD pattern of the compound $(Pr_{0.6}Sr_{0.4})_{0.95}$ $Fe_{0.8}Co_{0.2}O_{3-\delta}$ recorded in air at room temperature.

Figure 2. (Color online) Total conductivities as a function of temperature for the A-site deficient $(Pr_{0.6}Sr_{0.4})_{1-s}Fe_{0.8}Co_{0.2}O_{3-\delta}$ perovskites. The conductivity drops with increasing s. The conductivities have been corrected using the Bruggeman asymmetric model.[25]

samples were heated and cooled with a ramp of 5°C/min. The temperature range spanned was 50–1000°C. At every 50°C the samples were kept at temperature for 2 h. The resistance was measured every fifth minute. The characterizations of the cone-shaped electrodes were done in a setup described in Ref. 23. EIS was used to characterize the cone-shaped electrodes. The EIS was measured in the range of 1 MHz–0.05 Hz with five points measured at each decade. An amplitude of 36 mV was used throughout. An amplitude of 36 mV was needed to obtain data of sufficient quality. The measurements were done at 800, 700, and 600°C in the given order. The cones were equilibrated at temperature for 24 h before the measurements. 24 h were sufficient for equilibration. The measurements were done in air. For the EIS measurements a Solartron 1260 in stand-alone mode was used. The EIS data were treated in the PC-DOS program "equivcrt" by Boukamp.[24] Three (RQ) components were used in the fitting. Q is a constant phase element with the admittance

$$Y^* = Y_0(j\omega/\omega_0)^n \qquad [2]$$

where Y_0 is an admittance, ω is the angular frequency, j is the imaginary unit, and n is the frequency exponent.
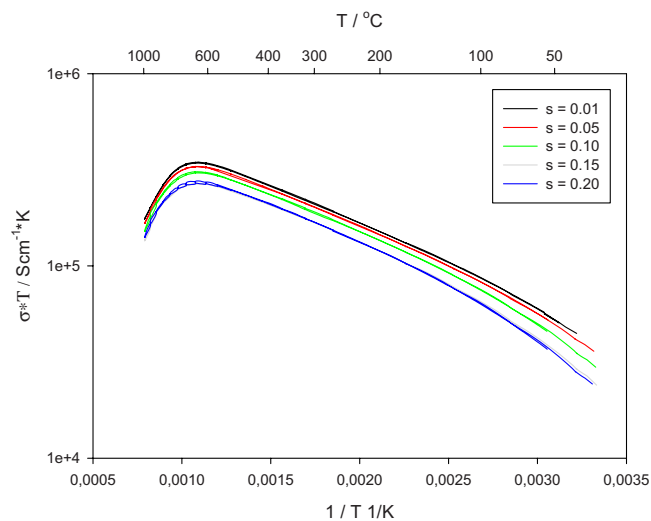
Results

A result from the powder XRD is found in Fig. 1. From powder XRD only the samples with $s=0.01$ and 0.05 are single phase. The

other samples contain an additional phase in the form of a Co–Fe-based spinel phase. As determined from XRD, the amount of the spinel phase increases with increasing s. The maximum amount of foreign phase is around 10% for $s = 0.2$. The unit cell parameters are found in Table I. The unit cell parameters show an irregular change with s. The peaks are rather broad. This is probably due to an inhomogeneous distribution of the cations. For the sintered bars a density in excess of 92% of the theoretical density was obtained.
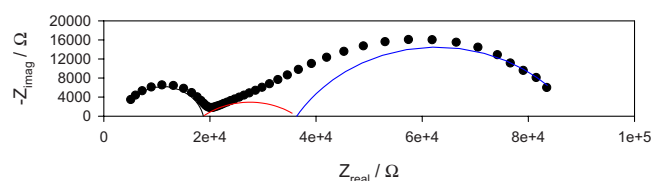
The results of the dilatometry measurements are found in Table II. Observe that the TEC decreases with decreasing stoichiometry on the A-site.

The conductivity of the samples is also dependent on the A-site stoichiometry. The conductivity as a function of temperature is plotted in Fig. 2. The conductivity is highest for the compound with $s = 0.01$ at all temperatures. For all the samples an increase in conductivity with an increase in temperature, until a certain temperature after which the conductivity decreases, is observed. The maximum in conductivity is found for the compound with $s = 0.01$, and it gives a value of 402 S cm^{-1} at 520°C.

An example of an EIS spectrum is seen in Fig. 3, together with the result of the fitting. The spectrum consists of three arcs. The variation in the total ASR with s at a temperature of 600°C is found in Fig. 4. The total ASR finds a minimum for the compound with $s=0.05$ with an ASR of 1.72 Ω cm^2 at 600°C. The total ASR values at the three measured temperatures are found in Table III. The contribution to the total ASR of the individual arcs at 600°C are found in Table IV, together with the n values. The n values are the frequency exponents given in Eq. 2.

Discussion

The A-site deficient $(Pr_{0.6}Sr_{0.4})_{1-s}Fe_{0.8}Co_{0.2}O_{3-\delta}$ perovskites differ from the A-site deficient $(La_{0.6}Sr_{0.4})_{1-s}Fe_{0.8}Co_{0.2}O_{3-\delta}$ perovskites.[15] In A-site deficient lanthanum-based perovskites, two perovskite phases are present along with a Fe–Co-based spinel

Table I. Unit cell parameters of A-site deficient $(Pr_{0.6}Sr_{0.4})_{1-s}Fe_{0.8}Co_{0.2}O_{3-\delta}$ perovskites measured with powder XRD in air at room temperature.

	s				
	0.01	0.05	0.10	0.15	0.20
A (Å)	7.717(10)	7.723(22)	7.723(6)	7.82(8)	7.711(9)
B (Å)	5.500(8)	5.47(3)	5.545(4)	5.455(14)	5.550(5)
C (Å)	5.448(5)	5.529(8)	5.484(5)	5.50(3)	5.504(8)

Table II. TEC values of A-site deficient $(Pr_{0.6}Sr_{0.4})_{1-s}Fe_{0.8}Co_{0.2}O_{3-\delta}$ perovskites in air from 100 to 900°C.

	s				
	0.01	0.05	0.10	0.15	0.20
TEC (10^{-6} K^{-1})	18.67 ± 0.2	18.23 ± 0.3	17.70 ± 0.3	17.35 ± 0.2	16.94 ± 0.2

Figure 3. (Color online) EIS of the compound $(Pr_{0.6}Sr_{0.4})_{0.90}Fe_{0.8}Co_{0.2}O_{3-\delta}$ at 600°C in air. Circles are measured data. Solid line is fitted data. Characteristic frequencies are marked.

phase. The two perovskites phases in the A-site deficient lanthanum-based perovskites are two phases with different amounts of La, Sr, Fe, and Co. In praseodymium-based perovskites, only one perovskite phase is present along with a Co–Fe-based spinel phase.

The variation in the TEC with *s* is systematic, as the TEC decreases almost linearly with increasing A-site deficiency. This is probably due to the impurities with the spinel phase, and because cobalt is lost from the perovskite phase[16] (Fe-based perovskites have much lower TEC than Fe–Co-based perovskites).[17] The change in TEC could also be due to a change in the point defect concentrations. The TEC values found for the A-site deficient Pr-based perovskites are higher than the TEC for CGO electrolytes.[26] However,
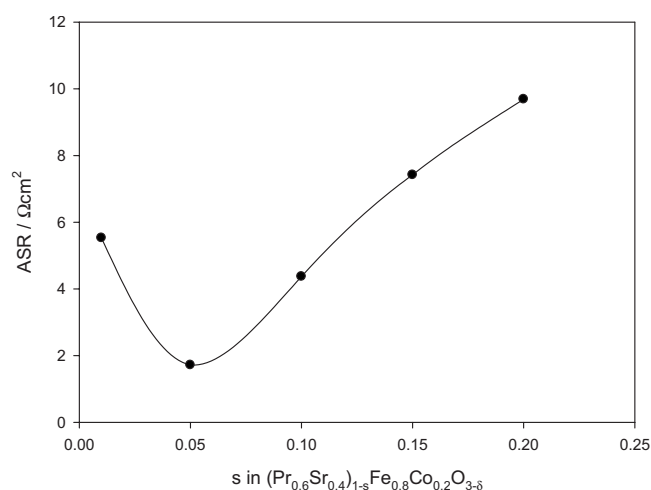
Figure 4. Total ASR values as a function of *s* measured in air at 600°C with EIS. The uncertainties on the contact areas are around 10–15%.

Table III. Total ASR values for A-site deficient $(Pr_{0.6}Sr_{0.4})_{1-s}Fe_{0.8}Co_{0.2}O_{3-\delta}$ at three different temperatures in air measured with EIS. The values are given in Ω cm².

	s				
	0.01	0.05	0.10	0.15	0.20
600°C	5.53	1.72	4.37	7.42	9.69
700°C	0.64	0.20	0.61	0.97	0.95
800°C	0.11	0.05	0.07	0.15	0.17

composite electrodes made by the A-site deficient perovskites and CGO might be of use as cathodes on a CGO electrolyte.

The electronic conductivity of the compounds changes from a metallic to a semiconductor-like behavior when the temperature is lowered, that is, the electronic conductivity increases until a certain temperature is reached after which the electronic conductivity decreases. The conductivity behavior as a function of temperature below a certain characteristic temperature indicates that the conductivity is due to the small polaron hopping mechanism[27] with the following relationship

$$\sigma = (A/kT^v)\exp(-E_a/kT) \qquad [3]$$

where *A* is a material constant, *k* is Boltzmann's constant, and E_a is the activation energy. The exponent *v* is 1 for the adiabatic small polaron hopping process and 3/2 for the nonadiabatic small polaron hopping process. The equation with $v=3/2$ fits the measured data best, in contrast to what has been observed by Tai et al.[28,29] but in agreement with Hansen and Hansen[15] for similar materials. The activation energy E_a of the total conductivity, below the temperature of maximum conductivity, is around 0.1 eV for all the compounds. The decrease in the total conductivity above a certain characteristic temperature can be explained as follows. When the temperature is increased, the perovskites lose oxygen. When oxygen vacancies are crested in the perovskite structure, a decoupling of the overlap between the d-orbitals of the transition metal and the p-orbitals of oxygen is the result. This can explain the lowered conductivity at high temperature.[28,29] Not only do the oxygen vacancies hinder the polaron hopping but they also alter the other defect concentrations which leads to a lowering of the concentration of charge carriers. This is the main effect. The calculated temperature of maximum conductivity is also higher than the observed temperature of maximum conductivity. The calculated temperature can be found using the equation

$$E_a = kT_{max} \qquad [4]$$

The calculated temperature of maximum conductivity is around 1150 K for all the compounds, compared to the observed temperature of maximum conductivity of approximately 800 K. This is also an indication that the oxygen stoichiometry is lowered upon heating of the perovskites. The conductivity behavior found in this study is almost the same as found in the literature.[13,15]

The variation in the total conductivity with *s* can be understood as follows. When *s* is increased, cobalt is lost from the perovskite phase, as observed for A-site deficient lanthanum-based perovskites[15] and confirmed by XRD. Fe–Co-based perovskites have a higher conductivity than Fe-based perovskites.[30] This therefore lowers the conductivity. Also, the presence of a spinel lowers the conductivity as Co–Fe-based spinels have a much lower conductivity than Fe–Co-based perovskites.[31]

Oxide ionic conductivity changes as a function of *s*. In the literature it was shown that a lowered A-site occupancy greatly influences the oxygen stoichiometry, oxygen ion vacancy, and cation vacancy concentrations for manganite-based perovskites.[32] However, no literature data on the defect chemistry of the A-site deficient Fe–Co-based perovskites have been given. In principle, a lowered A-site occupancy can lead to the creation of both oxide ion vacan-

Table IV. Contributions to the total ASR of the individual arcs for A-site deficient $(Pr_{0.6}Sr_{0.4})_{1-s}Fe_{0.8}Co_{0.2}O_{3-\delta}$ measured at 600°C in air with EIS. The values are given in Ω cm².

	s									
	0.01		0.05		0.10		0.15		0.20	
600°C	ASR	*n*	ASR	*n*	ASR	*n*	ASR	*n*	ASR	*n*
High	1.18	0.90	0.58	0.88	0.78	0.87	1.53	0.90	1.95	0.89
Medium	1.65	0.32	0.50	0.42	0.90	0.41	1.75	0.33	2.02	0.31
Low	2.70	0.78	0.64	0.98	2.69	0.64	4.14	0.66	5.72	0.67

Table V. Chemical capacitances of A-site deficient $(Pr_{0.6}Sr_{0.4})_{1-s}Fe_{0.8}Co_{0.2}O_{3-\delta}$ at 600°C in air measured with EIS.

	s				
	0.01	0.05	0.10	0.15	0.20
C_ω(low) (F cm^{-2})	0.089	0.15	0.16	0.042	0.20

cies and cation vacancies in the perovskite structure, but this has never been observed for perovskites; also, the powder XRD data suggest that excess Fe–Co is expelled from the perovskite structure when *s* is increased. If, however, both anion and cation vacancies are created in the perovskite structure, this probably lowers the oxide ionic conductivity due to the attraction between cation and anion vacancies.

The magnitude of the ASR is very high on cone-shaped electrodes compared to porous composite electrodes of the same materials. This is partly because cone-shaped electrodes are not composite electrodes, and partly due to the interface between the electrode–electrolyte, which is not optimized in the cone-shaped electrodes. The geometrical configuration of the cone-shaped electrode limits the number of contact points at the electrode–electrolyte interface. Also, the cone-shaped electrode is dense and therefore has a low surface area.

The interpretation of the EIS data can be done according to the mechanism suggested and confirmed by Siebert et al.[33] (We are well aware of other mechanisms suggested in the literature, but this mechanism fits the data best.) In this mechanism the high frequency arc is due to the exchange of oxide ions at the electrode–electrolyte interface. The equivalent capacity of this arc can be calculated using the equation[34]

$$C_\omega = R^{(1-n)/n}Y_0^{1/n} \qquad [5]$$

The magnitude of the equivalent capacity of this arc is between 0.5 and 1 µF cm^{-2} for all the compounds, suggesting that this arc is due to a double-layer effect.[35] The *n* values are all close to 0.9 for all the compounds, which again indicates that it is the same type of reaction that occurs on all the compounds. The medium frequency arc is normally attributed to the diffusion of oxide anions through the bulk of the electrode.[33] This arc finds its minimum for the compound with *s*=0.05, indicating that this compound has the highest oxide ionic conductivity. The magnitude of the low frequency arc is also dependent on *s*, the magnitude being smallest for the compound with *s*=0.05. The low frequency arc is due to a slow redox reaction at the surface of the electrode.[33] One possible explanation for this behavior could be the lowering of the surface segregation of A-site cations, increasing the amount of the catalytic active species Fe and Co on the surface of the electrode material. That the magnitude of the low frequency arc increases with a further decrease in *s* is perhaps due to the loss of cobalt from the perovskite phase. The equivalent capacity of this arc can be calculated for the high frequency arc using Eq. 5. The values are given in Table V. They all fall in the range for a chemical capacitance, as depicted in Ref. 36.

Furthermore it seems like the magnitude of the three arcs is coupled; they all decrease or increase in the same manner with a change in *s*. This parameter could either be the oxide ionic conductivity or the surface segregation of praseodymium, or perhaps both.

The electrochemical behavior of the A-site deficient Pr-based perovskites is markedly different from the behavior of the A-site deficient La-based perovskites. The effect of A-site deficiency is much less pronounced for the Pr-based perovskites than for the La-based perovskites.[8] This could be due to less surface segregation for the praseodymium-based perovskites than for the lanthanum-based perovskites. Praseodymium perhaps fits better in the perovskite structure than lanthanum, lowering the importance of A-site deficiency. It could also be due to the ability of praseodymium to

change its oxidation state. It could be that praseodymium has some catalytic activity in itself toward the reduction of oxygen. This has been shown for other systems.[37]

Conclusion

The TEC decreases almost linearly with *s*, probably due to the loss of cobalt from the perovskite phase. The total conductivity decreases as a function of increasing *s*. The effect of A-site substoichiometry on the activity of praseodymium-based perovskites toward the reduction of oxygen is reflected in a lowered ASR for the compound with *s*=0.05. This is thought to be due to lowering of the surface segregation of praseodymium.

References

1. N. Q. Minh, *J. Am. Ceram. Soc.*, **76**, 563 (1993).
2. J. M. Ralph, C. Rossignol, and R. Kumar, *J. Electrochem. Soc.*, **150**, A1518 (2003).
3. G. Xia and M. Liu, *Adv. Mater. (Weinheim, Ger.)*, **14**, 521 (2002).
4. C. Xia, W. Rauch, F. Chen, and M. Liu, *Solid State Ionics*, **149**, 11 (2002).
5. Y. Liu, W. Rauch, S. Zha, and M. Liu, *Solid State Ionics*, **166**, 261 (2004).
6. C. Xia and M. Liu, *Solid State Ionics*, **144**, 249 (2001).
7. Y. Liu, W. Rauch, S. Zha, and M. Liu, *Chem. Mater.*, **16**, 3502 (2004).
8. M. Sahibzada, S. J. Benson, R. A. Rudkin, and J. A. Kilner, *Solid State Ionics*, **113–115**, 285 (1998).
9. E. P. Murray, M. J. Sever, and S. A. Barnett, *Solid State Ionics*, **148**, 27 (2002).
10. Z. Shao and S. M. Haile, *Nature (London)*, **431**, 170 (2004).
11. A. Yan, M. Cheng, Y. Dong, W. Yang, V. Maragou, S. Song, and P. Tsiakaras, *Appl. Catal., B*, **66**, 64 (2006).
12. A. Yan, V. Maragou, A. Arico, M. Cheng, and P. Tsiakaras, *Appl. Catal., B*, **76**, 320 (2007).
13. G. Ch. Kostogloudis and Ch. Ftikos, *Solid State Ionics*, **126**, 143 (1999).
14. W. G. Wang and M. Mogensen, *Solid State Ionics*, **176**, 457 (2005).
15. K. K. Hansen and K. V. Hansen, *Solid State Ionics*, **178**, 1379 (2007).
16. S.-I. Hashimoto, K. Kammer, P. H. Larsen, F. W. Poulsen, and M. Mogensen, *Solid State Ionics*, **176**, 1013 (2005).
17. K. Kammer, L. Mikkelsen, and J. B. Bilde-Sørensen, *J. Solid State Electrochem.*, **10**, 934 (2006).
18. K. Kammer, *Solid State Ionics*, **177**, 1047 (2006).
19. S.-I. Hashimoto, K. Kammer, F. W. Poulsen, and M. Mogensen, *J. Alloys Compd.*, **428**, 256 (2007).
20. J. Newman, *J. Electrochem. Soc.*, **113**, 501 (1966).
21. I. Ruiz de Larramendi, D. G. Lamas, M. D. Cabezas, J. I. Ruiz de Larramendi, N. E. Walsöe de Reca, and T. Rojo, *J. Power Sources*, In press.
22. L. A. Chick, L. R. Pederson, G. D. Maupin, J. L. Bates, L. E. Thomas, and G. J. Exarhos, *Mater. Lett.*, **10**, 6 (1990).
23. M. Juhl, M. Mogensen, T. Jacobsen, B. Zachau-Christiansen, N. Thorup, and E. Skou, *Proceedings of the 4th International Symposium on Solid oxide fuel cells (SOFC-IV)*, Yokohama, June 18–23, M. Dokiya, O. Yamamoto, H. Tagawa and S. C. Singhal, Editors, The Electrochemical Society, Pennington, NJ, Vol. PV 95-1, p. 554 (1995).
24. B. A. Boukamp, *Solid State Ionics*, **20**, 31 (1986).
25. D. A. G. Bruggeman, *Ann. Phys.*, **416**, 636 (1935).
26. N. Kim, B.-H. Kim, and D. Lee, *J. Power Sources*, **90**, 139 (2000).
27. J. M. Wimmer and I. Bransky, in *Electrical Conductivity in Ceramics and Glass*, N. M. Tallan, Editor, Chap. 4, Pergamon, New York (1971).
28. L.-W. Tai, M. M. Nasrallah, H. U. Anderson, D. M. Sparlin, and S. R. Sehlin, *Solid State Ionics*, **76**, 259 (1995).
29. L.-W. Tai, M. M. Nasrallah, H. U. Anderson, D. M. Sparlin, and S. R. Sehlin, *Solid State Ionics*, **76**, 273 (1995).
30. M. V. Patrakeev, J. A. Bahteeva, E. B. Mitberg, I. A. Leonidov, V. L. Kozhevnikov, and K. R. Poeppelmeier, *J. Solid State Chem.*, **172**, 219 (2003).
31. D. S. Erickson and T. O. Mason, *J. Solid State Chem.*, **59**, 42 (1985).
32. F. W. Poulsen, *Solid State Ionics*, **129**, 145 (2000).
33. E. Siebert, A. Hammouche, and M. Kleitz, *Electrochim. Acta*, **40**, 1741 (1995).
34. T. Jacobsen, B. Zachau-Christiansen, L. Bay, and S. Skaarup, in *Proceedings of the 17th International Symposium on Materials Science*, F. W. Poulsen, N. Bonanos, S. Linderoth, M. Mogensen, and B. Zachau-Christiansen, Editors, Risø National Laboratory, p. 29 (1996).
35. N. L. Robertson and J. N. Michaels, *J. Electrochem. Soc.*, **138**, 1494 (1991).
36. S. B. Adler, J. A. Lane, and B. C. H. Steele, *J. Electrochem. Soc.*, **143**, 3554 (1996).
37. R. M. L. Werchmeister, K. K. Hansen, and M. Mogensen, To be published.